

NE533: MOOSE Project Part 3

Anthony Cowan

April 25, 2025

Department of Nuclear Engineering
North Carolina State University

Contents

1	Introduction	1
2	Methods	1
2.1	Steady-State Heat-Conduction Model	1
2.2	Mesh Convergence - Part 1	3
2.3	Transient Heat-Conduction Model	4
2.4	Temperature-Dependent Thermal Conductivity	4
2.5	Axially Varying Parameters	5
2.6	Mesh Convergence - Part 2	5
2.7	Burnup Effects	5
2.8	Mechanics	6
2.9	Constraints	7
2.10	Mesh Convergence - Part 3	7
3	Results and Discussion	7
3.1	Part 1 Mesh Convergence	7
3.2	1-D Steady State	7
3.3	1-D Transient	9
3.4	Mesh Convergence - Part 2	9
3.5	2-D Axially Varying Parameters	10
3.6	Mesh Convergence - Part 3	10
3.7	Gap Closure and Stress Profiles	11
4	Conclusion	11
5	Appendix	12

1 Introduction

The modeling and simulation of nuclear fuel performance is critical to ensuring the safety and efficiency of nuclear reactors. This project focuses on the steady-state and transient thermal and mechanical behavior of a fuel pellet system using the MOOSE (Multiphysics Object-Oriented Simulation Environment) framework. The objectives are distributed between three parts.

For part one, the required models are 1) a 1-D r-z steady-state, constant thermal conductivity system, 2) a 1-D r-z time-dependent, constant thermal conductivity system, and 3) a temperature-dependent thermal conductivity application to the previous two systems. The first requires a temperature profile to be reported, and the second demands a transient and peak centerline temperature.

Part two instructs the construction of the following model—a 2-D r-z, steady-state temperature-dependent thermal conductivity system with an axially varying heating rate and coolant temperature. The deliverables are axial temperature profiles for the fuel centerline, fuel surface, inner, and outer clad.

Finally, part three requires a 2-D mechanical treatment for the transient, temperature-dependent thermal conductivity model from part one, with the addition of a burnup dependency on the fuel thermal conductivity and a constant linear heating rate; effects of thermal expansion, densification, and fission-product-induced swelling are to be included. Results for gap width, burnup, average, and maximum stress are included.

The following report documents the approach and analysis of the stipulated problem statements, including the methods, results, and discussion of each part.

2 Methods

To obtain a final solution to the problem set, several steps were taken, including 1) the construction of a simple r-z steady-state model, 2) a mesh convergence study for the steady-state model, 3) adding transient capabilities to the steady-state model, 4) augmenting the thermal conductivity of all materials, in both the steady-state and transient cases, to rely on temperature-dependent empirical models, and 5) applying stipulated axial varying parameters and performing a mesh convergence study for this model.

2.1 Steady-State Heat-Conduction Model

The first step to establishing the steady-state model was defining geometric and material parameters. For the former, all parameters were taken from the problem definition. UO₂ fuel, helium gap, and zirconium cladding were selected to locate material properties. These parameters were found through differing sources; all thermophysical properties were found in the "Lecture 3" slide deck on slide 31 for the fuel and cladding. For the gap, it was assumed that it was a pure helium system; properties were found in an article that detailed a helium-related study^[3]. Table 1 outlines geometric parameters, and Table 2 details the located thermophysical properties. All material properties were put into the "Materials" block using "ADHeatConductionMaterial" and "ADGenericConstantMaterial".

Table 1: Geometric Parameters

Block	r _{min} (cm)	r _{max} (cm)	z (cm)
Fuel	0	0.5	1
Gap	0.5	0.505	1
Clad	0.505	0.605	1

Table 2: Thermophysical Properties

Properties	UO ₂	He	Zr
k _{th} (W/cm-K)	0.03	0.15 × 10 ⁻²	0.17
c (J/g-K)	0.33	5.19	0.35
ρ (g/cm ³)	10.98	0.18 × 10 ⁻³	6.50

The governing equation that is used to solve this problem is the heat conduction equation; the three-dimensional, transient form of the equation is defined as

$$\rho(t, \vec{x})c(t, \vec{x})\frac{\partial T}{\partial t} = \nabla \cdot [k(t, \vec{x})\nabla T(t, \vec{x})] + \dot{q} \quad (1)$$

Equation (1) can be simplified by applying some reasonable assumptions, the first being that the problem is spatially 2D (RZ). After this, Equation (1) becomes

$$\rho(t, r, z)c(t, r, z)\frac{\partial T}{\partial t} = \nabla \cdot [k(t, r, z)\nabla T(t, r, z)] + \dot{q} \quad (2)$$

The next assumption is that the system is steady-state or $\frac{\partial T}{\partial t} = 0$; Equation (2) becomes

$$0 = \nabla \cdot [k(r, z)\nabla T(r, z)] + \dot{q} \quad (3)$$

Finally, it is assumed that the thermal conductivity is a constant; this produces the following equation:

$$0 = k\nabla^2T(r, z) + \dot{q} \quad (4)$$

This second-order partial differential equation (PDE) requires at least two boundary conditions to be solved. The first is a Dirichlet boundary condition established by the problem statement, and the second is a zero-flux, reflective Neumann boundary condition at the centerline of the fuel pellet, imposing that only half of the geometry needs to be modeled. A zero-flux, reflective Neumann boundary condition was added to the top and bottom boundaries to produce a 1D calculation per the problem requirements. Our final equation definition now becomes

$$0 = k\nabla^2T(r, z) + \dot{q}$$

$$\nabla T(r, 0) = \nabla T(r, 1) = \nabla T(0, z) = 0, T(0.605, z) = 550 \quad (5)$$

The governing equation was implemented in MOOSE's "Kernels" block; the first term was added using the Heat Transfer Module types of "ADHeatConduction" and the second term with "HeatSource". The given linear heat rate (350 W/cm) had to be changed to a volumetric heat rate, taking its quotient with the surface area of the top face of the fuel; this calculation was placed in the "Functions" block as a "ParsedFunction", as shown in Equation (6).

$$\text{VHR} = \frac{\text{LHR}}{\pi R_f^2} \quad (6)$$

The boundary conditions were established in the "BCs" block using "ADDirichletBC" and "ADNeumannBC." The "Variables" block specified the variable "T" to inform MOOSE it should solve for that variable. The problem was designated as steady-state by specifying "type = Steady" in the "Executioner" block.

The temperature profile was probed by establishing a "VectorPostprocessor" using "LineValue-Sampler", which samples the variable, T, along a vector with a prescribed start and end point; this was chosen to span the entire radius of the fuel pellet at z=0.5 cm with 1000 sampling points.

All tolerances, solver, and preconditioning settings were selected through trial and error to produce a reasonable solution.

2.2 Mesh Convergence - Part 1

The "Mesh" block is the final piece required to complete the MOOSE input file. A single square mesh was created for simplicity, ranging from $0 \leq r \leq 0.605$ cm and $0 \leq z \leq 1$ cm. The coordinate system was set to "RZ" to keep calculations and boundary condition definitions consistent. The elements in the mesh were then assigned subdomain IDs associated with each material, as defined by their radius ranges, which are shown in Table 1, using "Subdomain-BoundingBoxGenerator".

A mesh convergence study was conducted to find a suitable mesh refinement for a reasonable solution. To quantify convergence, both a qualitative and an error assessment were performed, where the error is computed using the L2 norm, which is defined as

$$\|T\|_2 = \sqrt{(T^h - T)^2} \quad (7)$$

where T^h is the numerical solution generated by MOOSE and T is the analytic solution for the steady-state, constant k_{th} system, which is represented by

$$T_f(r) = T_g(0.5) + \frac{\text{VHR}(R_f^2 - r^2)}{4k_f} \quad (8)$$

$$T_g(r) = T_c(0.505) - \ln\left(\frac{r}{R_g}\right) \frac{\text{LHR}}{2\pi k_g} \quad (9)$$

$$T_c(r) = T_{oc} - \ln\left(\frac{r}{R_c}\right) \frac{\text{LHR}}{2\pi k_c} \quad (10)$$

$$T(r) = \begin{cases} T_f(r), & 0 \leq r \leq R_f \\ T_g(r), & R_f < r \leq R_g \\ T_c(r), & R_g < r \leq R_c \end{cases} \quad (11)$$

where T_f , T_g , and T_c are the analytical temperature profile solutions for the fuel, gap, and cladding, respectively; T_{oc} is the temperature established by the Dirichlet boundary condition; and VHR and LHR are the volumetric heat rate and linear heat rates. Note that this subscript notation remains consistent for any other material or geometric parameters shown in the equations above.

The convergence study began with $n_x = 75$ and $n_y = 1$, where each represents the number of divisions for the elements along their respective axes. The values were then doubled until a reasonable error margin was achieved. The final mesh specifications were also used for the transient and temperature-dependent models.

2.3 Transient Heat-Conduction Model

For the transient model, an assumption of a constant thermal conductivity was applied to Equation (2); this produces the following equation:

$$\rho(t, r, z)c(t, r, z)\frac{\partial T}{\partial t} = k\nabla^2T(t, r, z) + \dot{q} \quad (12)$$

A third kernel sub-block, "ADHeatConductionTimeDerivative," was added to account for the time-derivative term. The executioner type was changed to "Transient," and start and end times of 0 and 100 seconds were prescribed. "IterationAdaptiveDT" was also built in to allow for adaptive time-stepping according to an optimal number of non-linear solver iterations; this significantly reduced simulation time.

The final step was changing the LHR to a time-dependent form, shown in Equation (13), as stipulated by the problem.

$$\text{LHR} = 350 \exp\left(\frac{(t - 20)^2}{2}\right) + 350 \text{ W/cm} \quad (13)$$

2.4 Temperature-Dependent Thermal Conductivity

Equations (2) and (3) are revisited to account for temperature-dependent thermal conductivity. Empirical fuel and gap materials models were found in the "Lecture 3" slide deck on slides 15 and 26, respectively. A model for the cladding was found in literature^[1]; all of the models are presented below.

$$k_f = \frac{1}{100} \left[\frac{100}{7.5408 + 17.629t + 3.6142t^2} + \frac{6400}{t^{5/2}} \exp\left(\frac{-16.35}{t}\right) \right] \text{ W/cm - K} \quad (14)$$

$$k_g = 16 \times 10^{-6} T^{0.79} \text{ W/cm - K} \quad (15)$$

$$k_c = \frac{[8.8527 + 7.0820 \times 10^{-3} T + 2.5329 \times 10^{-6} T^2 + 2.9918 \times 10^3 T^{-1}]}{100} \text{ W/cm - K} \quad (16)$$

where $t = \frac{T}{1000}$. Each of the empirical models was integrated into the MOOSE file by adding them as a "ParsedFunction" in the "Functions" block and calling them using "thermal_conductivity_temperature_function" in the "ADHeatConductionMaterial" sub-blocks. Everything else remained consistent regarding the steady-state and transient models.

2.5 Axially Varying Parameters

As the problem statement outlines, two changes must be made to the steady-state model: 1) axial varying VHR and 2) axial varying coolant temperature. For the former, the VHR function can be changed to match the new conditions; Equation 17, found in the Lecture 3 slide deck on slide 39, outlines the expression used in the model, where LHR⁰ is the given LHR for the midpoint and Z₀ is the half-length of the rod. The Dirichlet boundary condition on the clad surface was changed to a FunctionDirichletBC type, allowing the Dirichlet BC to vary based on a prescribed function. Equation 18, created from equations found in the Lecture 3 slide deck on slides 33 and 40, outlines how to get cladding temperature from the prescribed coolant inlet temperature.

Note: MOOSE interprets z as y in the r-z coordinate system, so all z variables are replaced with y when translating to MOOSE.

$$\text{VHR}(z) = \frac{\text{LHR}^0 \cos \left[1.2 \left(\frac{z}{Z_0} \right) - 1 \right]}{\pi R_f^2} \quad (17)$$

$$\begin{aligned} T_{oc} &= T_{cool} + \frac{\text{LHR}(z)}{2\pi R_f h_{cool}} \\ &= T_{cool}^{in} + \frac{Z_0 \text{LHR}^0}{1.2 \dot{m} C_{pw}} \left\{ \sin(1.2) + \sin \left[1.2 \left(\frac{z}{Z_0} - 1 \right) \right] \right\} + \frac{\text{LHR}(z)}{2\pi R_f h_{cool}} \end{aligned} \quad (18)$$

Values for \dot{m} , C_{pw} , and h_{cool} were also found in the Lecture 3 slide deck on slides 33 and 41; these values are as follows: $\dot{m} = 250$ g/s, $C_{pw} = 4.2$ J/g-K, and $h_{cool} = 2.65$ W/cm²-K.

2.6 Mesh Convergence - Part 2

A mesh convergence study was performed on the number of divisions in the z-direction, as the convergence in the r-direction will already be captured by the analysis conducted for Part 1. Due to the absence of an analytical solution, convergence is considered reached when the peak centerline temperature has no significant change compared to the previous mesh in magnitude and axial position. Values of $n_y = 5, 10, 25, 50, 100, 200$, and 400 were used.

2.7 Burnup Effects

A fission rate, established by the system's power, was found to capture burnup. This was accomplished using the following equation:

$$\beta = \frac{\dot{F}t}{N_U} \quad (19)$$

where N_U is the number of uranium atoms in a cubic centimeter in UO₂ fuel, and \dot{F} is the fission rate, which is defined as

$$\dot{F} = \frac{\text{VHR}}{3.28451 \times 10^{-11} \text{J/fission}} \quad (20)$$

With burnup defined, the burnup-dependent k_{th} can be defined; in this case, the NFIR model was used, which is provided in slide 26 of the Lecture 8 slide deck.

$$k = (1 - R_f(T))k_{ph1}(T, \beta) + R_f(T)k_{ph2}(T, \beta) + k_{el}(T)$$

$$R_f(T) = \frac{1}{2} \left(1 + \tanh \left(\frac{T - 900}{150} \right) \right)$$

$$k_{ph1} = \frac{1}{9.592 \times 10^{-2} + 6.14 \times 10^{-3}\beta - 1.4 \times 10^{-5}\beta^2 + (2.5 \times 10^{-4} - 1.81 \times 10^{-6}\beta)T}$$

$$k_{ph2} = \frac{1}{9.592 \times 10^{-2} + 2.6 \times 10^{-3}\beta + (2.5 \times 10^{-4} - 2.7 \times 10^{-7}\beta)T}$$

$$k_{el} = 1.32 \times 10^{-2} \exp(1.88 \times 10^{-3}T)$$

2.8 Mechanics

The governing equation for the mechanics in this problem is

$$\nabla \cdot \sigma = 0 \quad (21)$$

The constitutive law is defined as

$$\sigma = C : (\epsilon - \epsilon^*) \quad (22)$$

where C is the elasticity tensor and ϵ is the total strain tensor, defined as

$$\epsilon = \epsilon^e + \epsilon^* \quad (23)$$

where ϵ^e is elastic strain and ϵ^* is eigenstrains. For this system, it is assumed that all materials are isotropic elastic, so only two independent parameters are required; in this case, the elastic modulus and Poisson ratio are utilized. Their respective values were found in the Lecture slides and are shown in Table 3.

The empirical eigenstrain relationships were all found in the lecture slides and are summarized below.

$$\epsilon_D = \Delta\rho_0 \left(\exp \left(\frac{\beta \ln 0.01}{C_D \beta_D} \right) - 1 \right) \quad (24)$$

$$\epsilon_{sfp} = 5.577 \times 10^{-2} \rho \beta \quad (25)$$

$$\epsilon_{gfp} = 1.96 \times 10^{-28} \rho \beta (2800 - T)^{11.73} \exp(-0.0162(2800 - T)) \exp(-17.8 \rho \beta) \quad (26)$$

where $\Delta\rho_0$ is the maximum densification, and β_D is the burnup at which densification halts; the former was chosen as 0.01 and the latter 0.005 FIMA. The thermal eigenstrains were handled by MOOSE's built-in thermal eigenstrain objects; all that needed to be provided were the thermal expansion coefficients, which were sourced from the lecture slides, shown in Table 3.

Table 3: Elastic Properties

Material	E (GPa)	ν	α (1/K)
UO_2	200.0	0.345	11×10^{-6}
Zircaloy	80.0	0.41	7.1×10^{-6}

2.9 Constraints

In part 3, the gap was removed as a block to remove possible artificial mechanical behavior. Two constraints were established to account for interactions between the fuel and clad without the gap block: 1) a thermal constraint to handle heat transfer across the gap, and 2) a mechanical constraint to handle contact between the two layers when gap closure is reached. A Lagrangian multiplier method was used for the former, and for the latter, a penalty method was used. A penalty value of 5×10^{12} was the most optimal.

2.10 Mesh Convergence - Part 3

A similar approach was used for mesh convergence as in part 2; the relative parameters chosen were gap closure time and maximum stress, which is hoop stress. A reflective boundary condition was utilized on the bottom face to improve computational efficiency. Mesh divisions of $n = 1, 5, 10, 15, 20, 25, 30$, and 50 were used to quantify convergence. The clad n_x parameter was a fifth of those shown to match the scale between the fuel and clad.

3 Results and Discussion

3.1 Part 1 Mesh Convergence

As shown in Figure 1a, the solution was computed starting with $n_x = 75$ and $n_y = 1$, and a reasonable solution was reached with $n_x = 600$ and $n_y = 8$. Beyond this value, diminishing returns were evident in the L2 norm, shown in Figure 1b, so these parameters were selected for all models. It is worth noting that the spike in error in the gap region likely stems from the significant discontinuity in the material properties compared to the surrounding blocks. A more satisfactory approach could involve separate meshing for each block, allowing for finer tuning of the element population.

3.2 1-D Steady State

The results from the steady-state simulations, including the constant- and temperature-dependent k_{th} cases, are outlined in Figure 2a. It was established that the constant k_{th} case agrees favorably with the analytical solution. Table 4 outlines each model's found temperatures at the centerline, fuel surface, inner clad, and outer clad.

3.2 1-D Steady State

3 RESULTS AND DISCUSSION

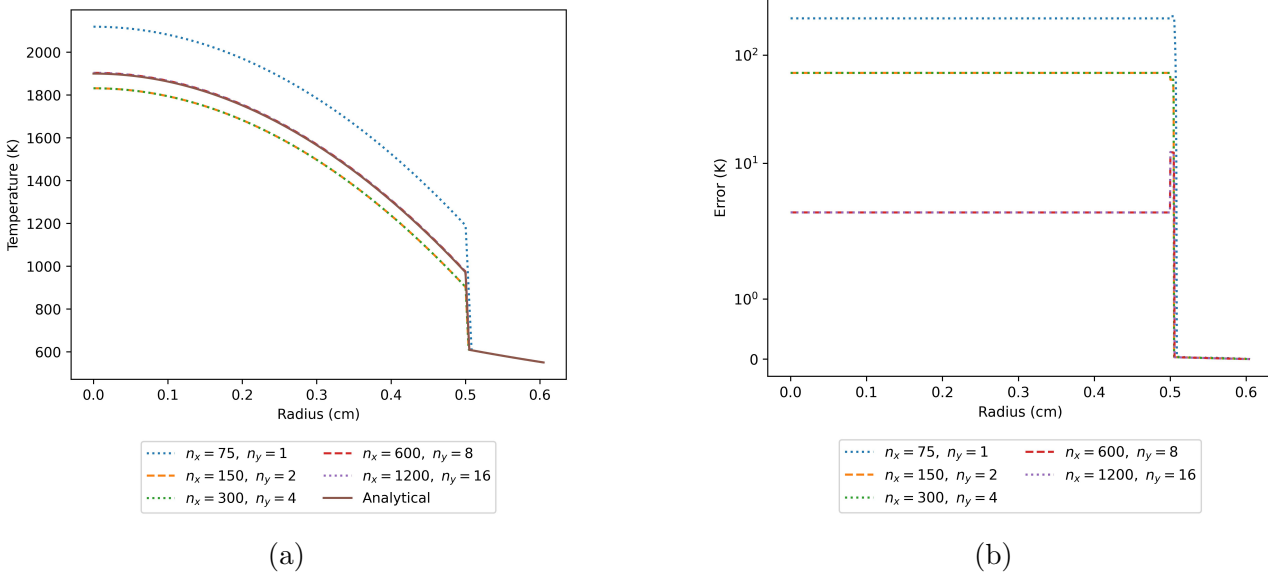


Figure 1: Part 1 Mesh Convergence Study Results (a) and Error from L2 norm (b)

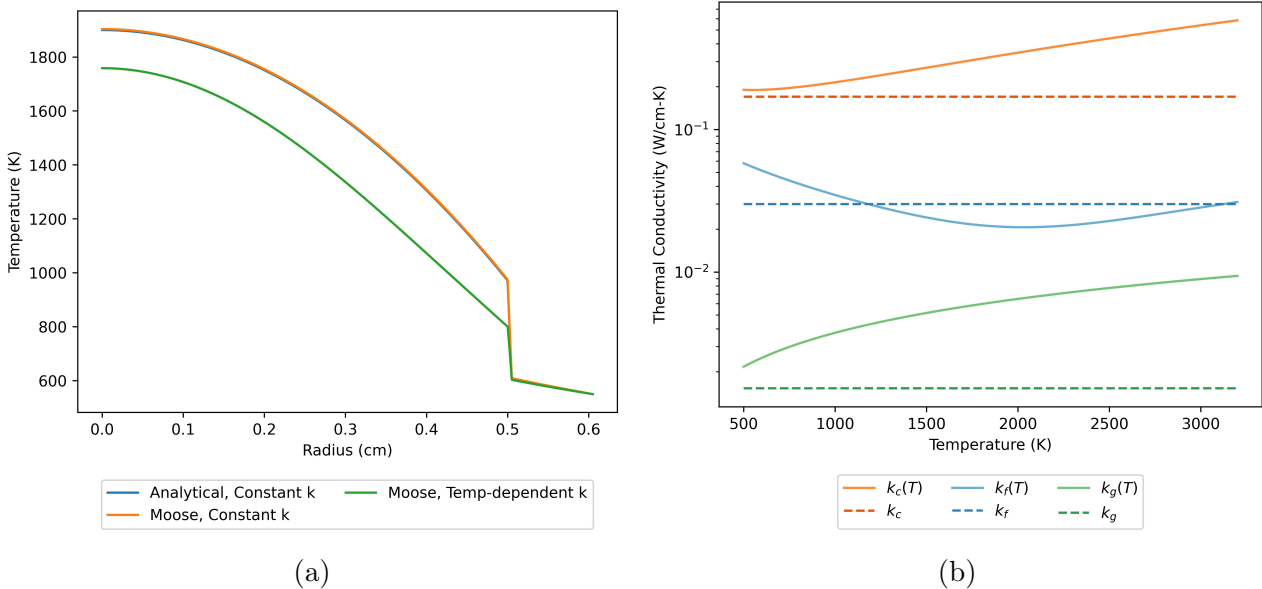


Figure 2: Steady-state temperature profiles (a) and temperature-dependent k_{th} functions (b)

Table 4: Steady State Temperatures at Interfaces

Model	T(0 cm)	T(0.5 cm)	T(0.505 cm)	T(0.605 cm)
Analytical	1899.88 K	971.47 K	608.20 K	550.00 K
Moose	1903.40 K	970.84 K	621.75 K	550.00 K
Moose $k_{th}(T)$	1758.43 K	798.63 K	610.45 K	550.00 K

3.3 1-D Transient

The results from the transient simulations, including the constant- and temperature-dependent k_{th} cases, are outlined in Figure 3a. The peak centerline temperature is 2102.02 K at 22.5 s for the constant- k_{th} model, and 2005.25 K at 23.2 s for the temperature-dependent- k_{th} model.

A plot of the LHR versus time is presented in Figure 3 to provide more context to the highly transient portion of Figure 3a between 20 and 40 seconds. The LHR is identical to the steady-state case after this transient event, so the centerline temperatures are expected to approach those in the steady-state case in this timeframe. This anticipation is confirmed as the centerline temperatures are visually the same between Figures 2a and 3a.

The general decrease in temperature is also observed here, which follows the logic established in the steady-state model as the temperature range is still valid.

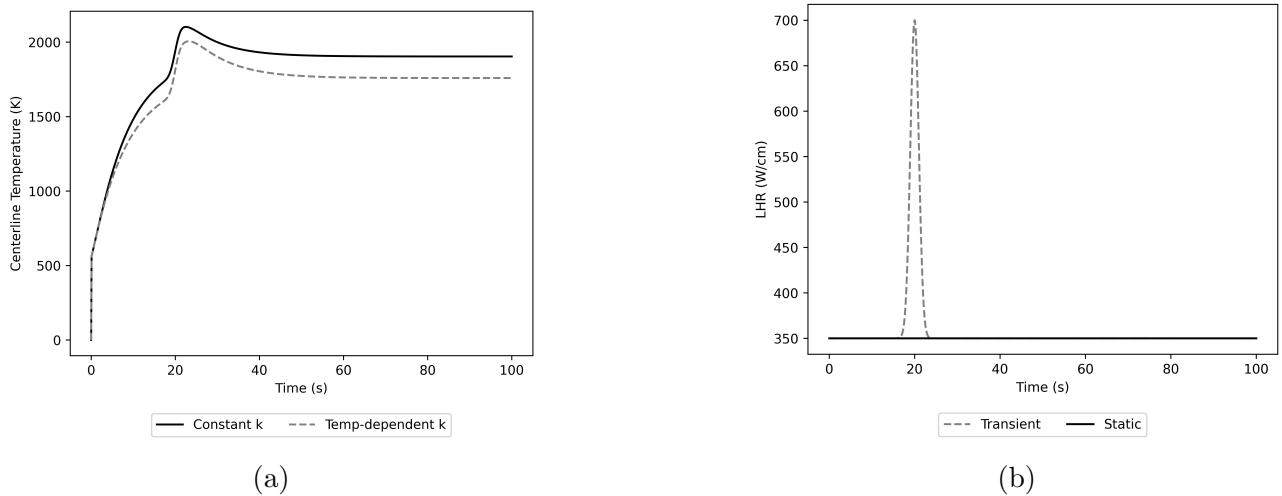


Figure 3: Transient centerline temperature vs time (a) and LHR temporal evolution (b)

3.4 Mesh Convergence - Part 2

As shown in Figure 4, the solution was computed starting with $n_y = 5$ and a reasonable solution was reached with $n_y = 200$.

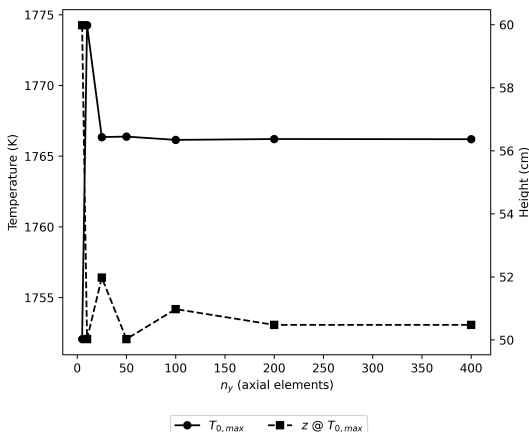


Figure 4: Part 2 Mesh Convergence Study Results

3.5 2-D Axially Varying Parameters

Figure 5 shows the axial temperature profile results. These shapes align closely with what is established in the literature^[2], as shown in Figure 8. Quantitative differences likely arise due to differences in material parameters. The peak centerline temperature is 1752.06 K and occurs at $z = 50.58$ cm.

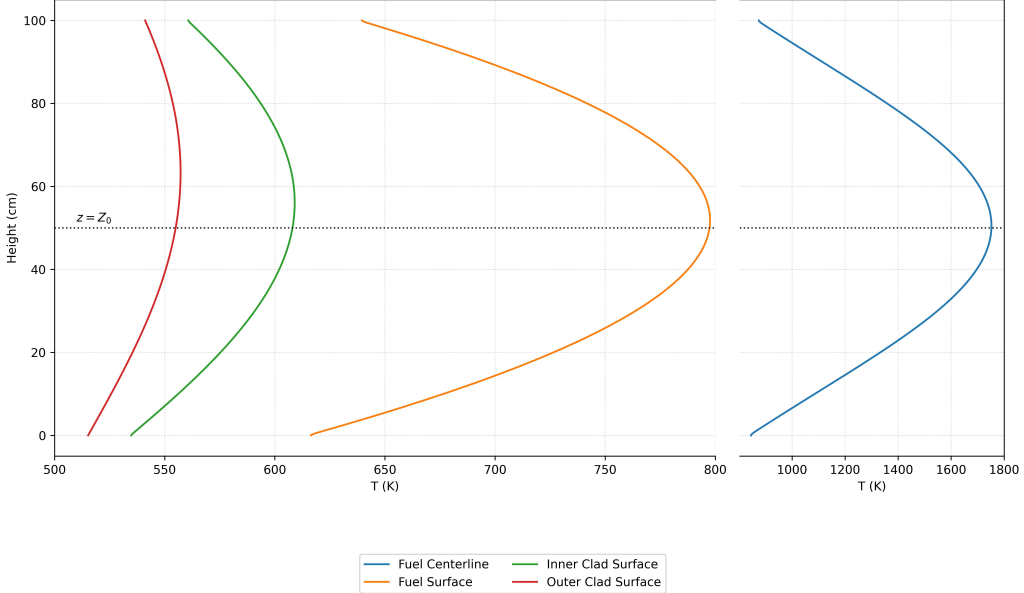


Figure 5: Axial temperature profiles at interfaces

3.6 Mesh Convergence - Part 3

As shown in Figure 6, the solution was computed starting with $n = 1$ and a reasonable solution was reached with $n = 30$.

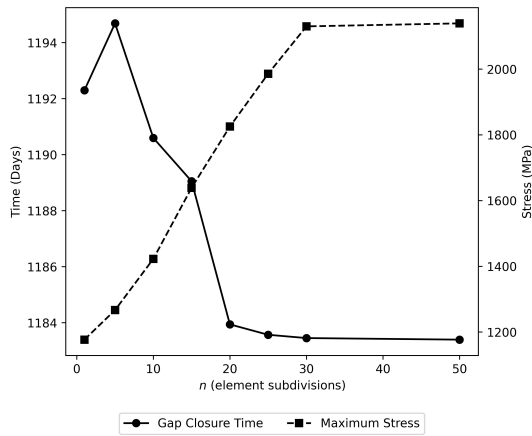


Figure 6: Part 3 Mesh Convergence Study Results

3.7 Gap Closure and Stress Profiles

Figure 7 shows the gap closure and burnup as a function of time along with the time-dependent stress profiles for average radial, axial, hoop, and maximum stress. The gap closure plot qualitatively agrees with the plots provided in Lecture 7 shown in Figure 9. Gap closure occurs around 1184 days.

As shown in figure 7b, the maximum stress exceeds the fracture stress, indicated by the dashed gray line, almost immediately. If cracking behavior were included in this model, cracks would form to relieve these high stresses. Using the ODE solution provided in the Lecture 6 slides, one can calculate the extent to which the cracks propagate, assuming no stress is coming from other eigenstrains; in this case, this is okay due to burnup being very small. After performing these calculations, with a $\Delta T = 600$, the cracks will extend radially about halfway into the fuel.

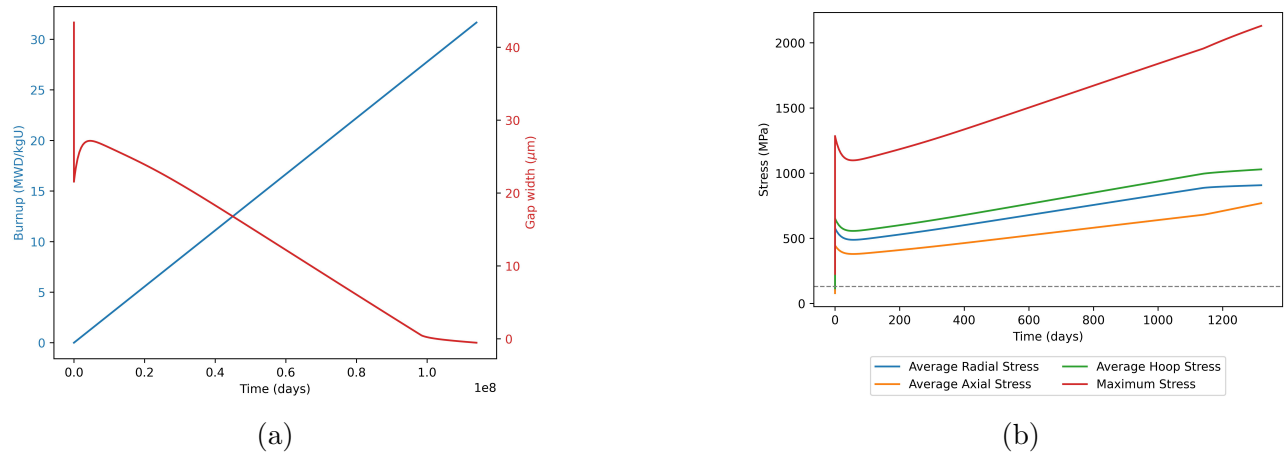


Figure 7: Gap width and burnup vs time (a) and stress profile temporal evolution (b)

4 Conclusion

This project demonstrates the MOOSE framework's effectiveness for simulating thermal behavior in nuclear fuel rods under steady-state and transient conditions. A mesh refinement of $n_x=600$, $n_y=8$ was found to balance accuracy and efficiency for Part 1, $n_y=200$ for the axially varying Part 2 case, and $n = 30$ for Part 3.

The steady-state constant- k_{th} model closely matched the analytical solution, while the temperature-dependent model exhibited lower peak temperatures. Transient results confirmed expected physical behavior, with temperatures stabilizing after the heat pulse. Axially varying VHR and coolant profiles produced temperature distributions consistent with the literature.

The mechanical model matched the qualitative behavior of the provided materials in the lecture slides. Gap closure occurred at 1184 days, and cracks would propagate about halfway through the fuel if they were to be modeled.

Future efforts include adding more complexities to the model to capture more accurate fuel behavior.

References

- [1] JK Fink and L Leibowitz. Thermal conductivity of zirconium. *Journal of Nuclear Materials*, 226(1-2):44–50, 1995.
- [2] Neil E Todreas and Mujid S Kazimi. *Nuclear systems volume I: Thermal hydraulic fundamentals*. CRC press, 2021.
- [3] Jiaping Yang, Cheng Peng Tan, and Eng Hong Ong. Heat transfer enhancement by helium gas filled in a hard disk drive enclosure. In *ASME International Mechanical Engineering Congress and Exposition*, volume 44281, pages 155–159, 2010.

5 Appendix

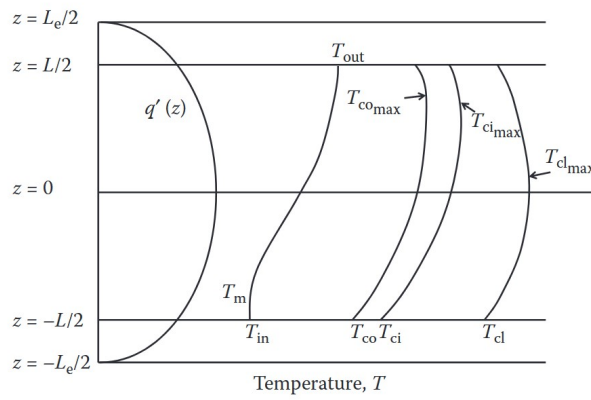


Figure 8: Typical shapes of axial temperature profiles for a UO₂ fuel rod with water coolant and constant k_{th} ^[2]

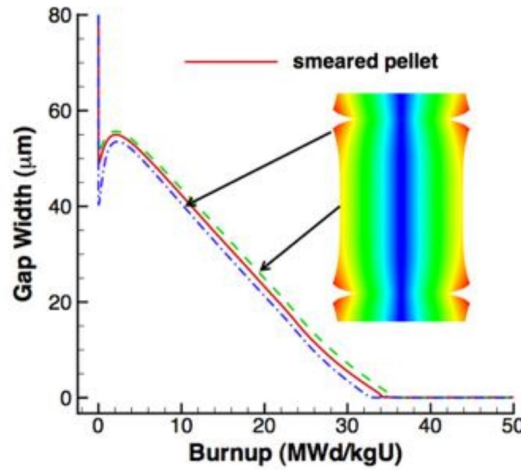


Figure 9: Gap width vs burnup for a smeared pellet.